# Molecular Orientation Distributions in a Biaxially oriented Poly(L-lactic Acid) Film Determined by Polarized Raman Spectroscopy

Masakazu Tanaka and Robert J. Young*

*Materials Science Centre, School of Materials, The University of Manchester, Grosvenor Street, Manchester, M1 7HS United Kingdom*

*Received April 3, 2006; Revised Manuscript Received July 20, 2006*

Molecular orientation distributions in the crystalline and amorphous regions of a biaxially oriented poly(L-lactic acid) film were analyzed fully by polarized Raman spectroscopy. Raman bands at 926 and 875 $cm^{-1}$ were chosen for the determination of the most probable molecular orientation distribution functions for the crystalline and amorphous regions in the film. It was revealed that the PLLA molecules were oriented biaxially in both the crystalline and amorphous regions. The orientation distribution normal to the film surface was found to be broader in the amorphous regions than in the crystalline regions. Furthermore, a predominant unidirectional molecular orientation was observed in the crystalline regions, whereas the molecular orientation distribution in the amorphous regions was isotropic in the plane parallel to the film surface. The different behavior of the crystalline and amorphous regions suggests that each region underwent different deformation mechanisms during the film formation.

## 1. Introduction

Poly(L-lactic acid) (PLLA) is well-known as a biomaterial owing to its biosorbable and biocompatible capabilities. PLLA is also an environmentally friendly compostable material and, hence, is processed into fibers and oriented films for a number of applications. The physical properties of oriented PLLA materials[1,2] are related closely to aspects of their microstructure such as their degree of crystallinity and molecular orientation. Recent studies have shown that the degradation rates of PLLA films are dependent on both the degree of crystallinity[3] and the presence of biaxial orientation[4] as well as the morphology of the film surface.[5] In addition, the degree of biaxial orientation in a polymer film is known to affect its barrier properties.[6,7]

The degree of crystallinity of semicrystalline polymers can be measured simply by thermal analysis or by wide-angle X-ray diffraction (WAXD), which can also give an indication of crystallite orientation. On the other hand, polarized Raman spectroscopy[8−10] has been regarded as a powerful technique to quantify the molecular orientation distributions, since it is capable of obtaining the fourth-order molecular orientation distribution coefficients as well as the second-order coefficients. The technique also enables the molecular orientation distributions in both the crystalline and amorphous regions of a polymer to be determined independently.[11−14]

Polarized Raman spectroscopy has been used mainly for the study of molecular orientation distributions in uniaxially oriented materials.[10−16] Since only a small number of the distribution coefficients have to be determined, polarized Raman scattering intensities can be measured for the backscattering (BS) geometry only. Meanwhile, only a few publications[17−19] have employed the technique for the study of molecular orientation distributions in biaxially oriented materials, where the scattering intensities have to be measured for the right-angle scattering (RAS) geometry as well as the BS geometry to determine all of the coefficients. The number of the coefficients to quantify the biaxial orientation distributions can, however, be reduced[20] by using Raman bands for which their tensors have cylindrical symmetry.

**Table 1.** Film Thickness Measurements and Thermal Characteristics[a] of the Biaxially oriented PLLA (BO−PLLA) Film

| | BO−PLLA |
|---|---|
| film thickness [$\mu$m] | 26.2 ± 0.8 |
| glass transition temperature [°C] | 64 |
| melting point [°C] | 167 |
| crystallinity ($\chi_c$) [%] | 38 |

[a] Determined by differential scanning calorimetry.

In the present investigation, molecular orientation distributions in a biaxially oriented poly(L-lactic acid) (PLLA) film have been studied using polarized Raman spectroscopy for the BS geometry only. The Raman bands of PLLA are assumed to be cylindrically symmetric[20] owing to its helical molecular structure.[21] A Raman band of PLLA at 926 $cm^{-1}$ was found[14] to be assigned to the crystalline regions only of PLLA, whereas another band at 875 $cm^{-1}$ was assigned to both the crystalline and amorphous regions. These Raman bands were chosen for the study of molecular orientation distributions in both the crystalline and amorphous regions, and the results have been compared with those obtained by WAXD and birefringence measurements.

## 2. Experimental Section

**2.1. Materials.** A biaxially oriented PLLA (BO−PLLA) film, Ecologe, was kindly supplied by Mitsubishi Plastics. The film thickness measurements and thermal characteristics of the sample are summarized in Table 1. The film thickness was determined from averaging nine independent samples using a micrometer. The glass transition temperature, melting temperature, and the heat of fusion of the film were determined by differential scanning calorimetry from two replicated measurements. The degree of crystallinity of the sample was determined

* To whom correspondence should be addressed. Tel: +44-161-306-3551. Fax: +44-161-306-3586. E-mail: robert.young@manchester.ac.uk.

10.1021/bm060326l CCC: $33.50 
Published on Web 08/23/2006

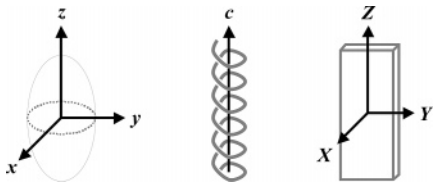


**Figure 1.** Definitions of the coordinates for a Raman polarizability tensor ($x-y-z$), the molecular chain axis ($c$), and the sample ($X-Y-Z$).

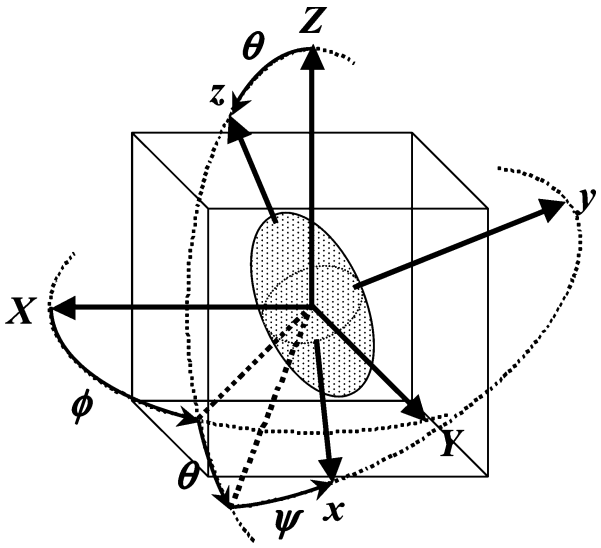


**Figure 2.** Angular relationships between the $x-y-z$ Raman polarizability tensor axes and the $X-Y-Z$ sample axes: azimuthal angle $\phi$, polar angle $\theta$, and rotational angle $\psi$.

from its heat of fusion using a reference value of 93.3 J/g for the melting of a PLLA single crystal with an infinite size.[22]

**2.2. Methods. 2.2.1. Polarized Raman Spectroscopy.** As shown in Figure 1, the principal axes for a Raman polarizability tensor and those for a sample were defined as $x-y-z$ and $X-Y-Z$ axes, respectively, throughout the current study.

Figure 2 shows the angular relationships between the $x-y-z$ Raman polarizability tensor axes and the $X-Y-Z$ sample axes, where angles $\phi$, $\theta$, and $\psi$ are azimuthal, polar, and rotational angles, respectively.

For a Raman polarizability tensor with a cylindrical symmetry around the $z$ axis ($\psi = 0$), its orientation distributions in a material can be explained mathematically by the following function:[8,23,24]

$$N(\phi,\theta) = \sum_{l=0}^{\infty} \sum_{m=-l}^{l} P_{lm0,\mathrm{chain}} Z_{lm0}(\cos\theta) \mathrm{e}^{-im\phi} \qquad (1)$$

where $P_{lm0,\mathrm{chain}}$ is the molecular orientation distribution coefficient and $Z_{lm0}(\cos\theta)$ is an expansion coefficient.

The polarized Raman scattering intensity depends on the angles between the principal axes of the Raman polarizability tensor and the direction of light polarization. The coefficient $P_{lm0,\mathrm{chain}}$ can be related to the Raman scattering intensities for different polarization scattering geometries by

$$\sum \alpha'_{g'g}\alpha'_{p'p} = \frac{N_\mathrm{o}}{4\pi^2} \sum_{lm0} \sqrt{\frac{2l+1}{2}} N_{lm0} P_{lm0,\mathrm{tensor}} A_{lm0}{}^{g'gp'p} \qquad (2)$$

where $\sum \alpha'_{g'g}\alpha'_{p'p}$ is a quadratic representation of the polarized Raman scattering intensity, $N_\mathrm{o}$ is a term related to the scattering volume, $N_{lm0}$ is a constant for order $lm0$,[17,23] $P_{lm0,\mathrm{tensor}}$ is the orientation distribution coefficient for the Raman polarizability tensor, and $A_{lm0}{}^{g'gp'p}$ is a term related[8] to the components of the tensor. The coefficient $P_{lm0,\mathrm{tensor}}$ can be related to the coefficient $P_{lm0,\mathrm{chain}}$ using the following relationship:[25,26]

$$P_{lm0,\mathrm{chain}} = \frac{P_{lm0,\mathrm{tensor}}}{P_{l00}(\cos\Omega)} \qquad (3)$$

where the function $P_{l00}(\cos\Omega)$ is a Legendre polynomial function of order $l00$ for the parameter cos $\Omega$. The angle $\Omega$ is the so-called tilt angle, which is the angle between the principal axis of the Raman tensor, $z$ axis, and that of a molecular chain, $c$ axis, as defined in Figure 1. The tilt angle has been determined[14] to be 0° and 44° for the Raman bands at 926 and 875 cm$^{-1}$, respectively.

Considering the cylindrical symmetry of the Raman bands of PLLA, eq 2 gives[20] six unknown parameters: $N_\mathrm{o}$, $P_{200}$, $P_{220}$, $P_{400}$, $P_{420}$, and $P_{440}$. These parameters can be determined by measuring the polarized Raman scattering intensities for six independent scattering geometries.

The six independent scattering geometries can be achieved for the BO−PLLA film if the polarized Raman spectra are collected in the directions along its principal $X$, $Y$, and $Z$ axes as defined in Figure 1; the $Z$ axis is in the direction parallel to the preferential molecular orientation direction in the film, the $X$ axis is normal to the film surface, and the $Y$ axis is perpendicular to both the $X$ and $Z$ axes. Hereafter, the polarized scattering geometry will be described using Porto's notation,[27] $A(BC)A$, where $A$ is the propagation direction of the incident and scattered light and $B$ and $C$ are the polarization directions of the incident and scattered light, respectively.

The BO−PLLA film was mounted directly on the sample stage so as to obtain the polarized Raman spectra for geometry $X(BC)X$ (through). The polarized Raman spectra for geometries $Y(BC)Y$ (edge) and $Z(BC)Z$ (end), on the other hand, were obtained from the film embedded in a cold-cured epoxy resin (Epofix, Struers), whose surface was mirror-polished in the direction normal to the $Y$ axis or $Z$ axis, respectively. Different sets of polarized Raman spectra were obtained from each sample by changing the polarization directions of the incident light and analyzed light, either to the horizontal or vertical direction in the projection plane, as summarized in Table 2. The table shows that polarized Raman scattering intensities $\sum \alpha'_{XX}{}^2$, $\sum \alpha'_{YY}{}^2$, and $\sum \alpha'_{ZZ}{}^2$ are measurable from two samples, although the values may not be identical due to differences in their Raman scattering volumes. The effect was, therefore, corrected by following the calculations described in the Appendix in order to determine the polarized Raman scattering intensities for the different polarization scattering geometries.

**Table 2.** Combinations of the Polarized Scattering Geometries Used for the Measurements of Raman Scattering Intensities in the BO−PLLA Film

| | sample section (projection plane) | | |
|---|---|---|---|
| direction of polarizer-analyzer[a] | through ($Y-Z$) | edge ($X-Z$) | end ($X-Y$) |
| H−H | $\sum \alpha'_{ZZ}{}^2$ | $\sum \alpha'_{ZZ}{}^2$ | $\sum \alpha'_{YY}{}^2$ |
| H−V | $\sum \alpha'_{YZ}{}^2$ | | $\sum \alpha'_{XY}{}^2$ |
| V−V | $\sum \alpha'_{YY}{}^2$ | $\sum \alpha'_{XX}{}^2$ | $\sum \alpha'_{XX}{}^2$ |
| V−H | | $\sum \alpha'_{ZX}{}^2$ | |

[a] H, horizontal; V, vertical in the projection plane.

The values $P_{lm0}$ for the crystalline regions, $P_{lm0,\mathrm{c}}$, can be determined[14] from the polarized Raman scattering intensities for the 926 cm$^{-1}$ band of PLLA after the correction for its tilt angle in eq 3. Similarly, the Raman band at 875 cm$^{-1}$ is useful[14] for the determination of the values $P_{lm0}$ averaged over the crystalline and amorphous regions ($P_{lm0,\mathrm{chain}}$).

Once both the values $P_{lm0,\mathrm{c}}$ and $P_{lm0,\mathrm{chain}}$ are known, the values $P_{lm0}$ for the amorphous regions only can be calculated[19] by the following equation assuming a simple two-phase model:

$$P_{2m0,\mathrm{a}} = \frac{1}{1-\chi_\mathrm{c}}(P_{2m0,\mathrm{chain}} - \chi_\mathrm{c} P_{2m0,\mathrm{c}}) \qquad (4)$$

for order $l = 2$. If the $P_{200,a}$ value is positive, the $P_{400,a}$ value may be estimated[28] from the $P_{200,a}$ value by

$$P_{400,a} = \frac{P_{200,a}(5P_{200,a} - 2)}{5 - 2P_{200,a}} \quad (5)$$

Except for samples with extremely high levels of molecular orientation in the amorphous regions, the values $P_{420,a}$ and $P_{440,a}$ are considered to be small,[29] and their influence on the function $N(\phi, \theta)$ in eq 1 for the amorphous regions may be assumed to be negligible compared to the influence of the values $P_{200,a}$, $P_{220,a}$, and $P_{400,a}$. To determine the function $N(\phi, \theta)$, however, neglecting the values $P_{lm0}$ for orders $l \geq 6$ may cause a considerable error.

This error can be reduced by replacing the function $N(\phi, \theta)$ with the most probable molecular orientation distribution function,[16,18,29] $N_{mp}(\phi, \theta)$, in the following equation:

$$N_{mp}(\phi,\theta) = \frac{\exp[\sum_{l,m} A_{lm0}^{mp} P_{lm0}(\cos\phi, \cos\theta)]}{\int_0^{\pi}\int_0^{2\pi} \exp[\sum_{l,m} A_{lm0}^{mp} P_{lm0}(\cos\phi, \cos\theta)] \sin\theta \, d\phi \, d\theta} \quad (6)$$

where the coefficients $A_{lm0}^{mp}$ were calculated by approximating eq 6 as

$$N_{mp}(\phi,\theta) = \frac{\exp[\sum_{l,m} A_{lm0}^{mp} P_{lm0}(\cos\phi, \cos\theta)]}{\sum_{\theta=0°}^{90°}\sum_{\phi=0°}^{90°} \exp[\sum_{l,m} A_{lm0}^{mp} P_{lm0}(\cos\phi, \cos\theta)] \sin\theta} \quad (7)$$

under a constraint of

$$P_{lm0} = \frac{\sum_{\theta=0°}^{90°}\sum_{\phi=0°}^{90°} N_{mp}(\phi,\theta) P_{lm0}(\cos\phi, \cos\theta) \sin\theta}{\sum_{\theta=0°}^{90°}\sum_{\phi=0°}^{90°} N_{mp}(\phi,\theta) \sin\theta} \quad (8)$$

The summations in eqs 7 and 8 were calculated in increments of angles $\phi$ and $\theta$ of 2°. It was difficult to determine all of the five variables $A_{200}^{mp}$, $A_{220}^{mp}$, $A_{400}^{mp}$, $A_{420}^{mp}$, and $A_{440}^{mp}$ simultaneously. Since the values $A_{420}^{mp}$ and $A_{440}^{mp}$ are considered to be small relative to the other variables,[19] the values $A_{200}^{mp}$, $A_{220}^{mp}$, and $A_{400}^{mp}$ were calculated initially assuming that the values $A_{420}^{mp}$ and $A_{440}^{mp}$ were zero. In the second step, the values $A_{420}^{mp}$ and $A_{440}^{mp}$ were calculated by using the values $A_{lm0}^{mp}$ determined in the first step. The error for the calculation, $R_A$, is defined by

$$R_A = \frac{1}{n_A} \sum_{l,m=0,2,4} \left| \frac{P_{lm0,\,exp} - P_{lm0,calc}}{P_{lm0,exp}} \right| \quad (9)$$

where $n_A$ is the number of the values $A_{lm0}^{mp}$ considered in the calculation. Coefficients $P_{lm0,exp}$ and $P_{lm0,calc}$ are the values $P_{lm0}$ determined by polarized Raman spectroscopy and by the calculation using eqs 7 and 8, respectively.

A Raman spectrometer (Raman Imaging Microscope System 1000, Renishaw) equipped with a near Infrared laser ($\lambda = 785$ nm, 22 mW output) was used to collect Raman scattering. Polarization filters and half-wave plates were fitted to control the polarization directions of incident and scattered light. A ×50 objective lens with a numerical aperture of 0.75 was used to focus the beam on the sample, assuming that the effect of polarization scrambling due to the lens is insignificant for the sample with small birefringence.[9,30−32] The system was calibrated for the peak position and scattering intensity using a silicon single crystal and liquid carbon tetrachloride, respectively, prior to the experiment. The spectra were analyzed using analytical software (GRAMS/32, Galactic), and each Raman band was fitted to a Gaussian−Lorentzian curve[12] to improve the accuracy of the intensity measurement.

The molecular orientation distribution coefficients for the crystalline ($P_{lm0,c}$) and amorphous regions ($P_{lm0,a}$) of the PLLA film were determined from the set of the polarized Raman scattering intensities given in Table 2. The polarized Raman scattering intensity for each scattering geometry was determined by averaging 5 independent spectra in the same region in the sample. Two independent films were studied to confirm the reproducibility of the data.

**2.2.2. Wide-Angle X-ray Diffraction.** The orientation distributions of the crystallites, which are considered to be equivalent to the molecular orientation distributions in the crystalline regions, were determined by WAXD. Two different techniques were employed to measure the distributions in the $X-Z$ and $Y-Z$ planes of the BO−PLLA film. PLLA is known to have different crystal forms,[21,33] and only the α-form crystal, which is the most common form, was observed for the samples in the current study.

The distribution in the $X-Z$ plane of the sample was studied from $\theta$-offset profiles using an X-ray diffractometer (X'Pert PW 3040/00, Philips). Ni-filtered Cu Kα radiation was chosen for the analysis using an excitation condition of 50 kV and 40 mA. In the symmetrical-transmission geometry, the diffraction intensities for the (0 0 10) plane of the PLLA α-form crystal were recorded for $\theta$-offset angles between ±15° in increments of 1°.

The distribution in the $Y-Z$ plane of the sample was studied using an X-ray flat plate camera. An X-ray generator (PW 1120/90, Philips) fitted with Ni-filtered Cu Kα radiation (40 kV, 40 mA) was employed to record the diffraction pattern on a film negative. The film negative was scanned using a commercial scanner (Scan Jet ADF, Hewlett-Packard) and analyzed using analytical software[34] (Fit2D Ver. 10.95, ESRF). Diffraction arcs for the (2 0 0)/(1 1 0) planes of PLLA α-form crystal were analyzed[14] to determine the orientation distribution of the crystallite chains, since diffraction arcs for the (0 0 10) plane of the PLLA film were found to be overlapped with those for the (1 0 10) plane.

The distribution function of the diffraction intensity in the $X-Z$ plane, $I_c(\theta_{XZ})$, may be equivalent to the distribution of molecular chains in the crystallites, since the normal vector for the (0 0 10) plane is in the direction parallel to the crystallite chain axis ($c$ axis). Similarly, the distribution function of the crystallite chain axis in the $Y-Z$ plane is defined as $I_c(\theta_{YZ})$. Both the functions $I_c(\theta_{XZ})$ and $I_c(\theta_{YZ})$ are normalized to

$$\sum_{\theta_{XZ}=-90°}^{90°} I_c(\theta_{XZ}) = \sum_{\theta_{YZ}=-90°}^{90°} I_c(\theta_{YZ}) = 1 \quad (10)$$

The two-dimensional parameters $I_c(\theta_{XZ})$ and $I_c(\theta_{YZ})$ may be combined to obtain a three-dimensional orientation distribution of PLLA crystallites in the BO−PLLA film, $I_c(\phi, \theta)$, by

$$I_c(\phi,\theta) = I_c(\theta_{XZ}) I_c(\theta_{YZ}) \quad (11)$$

where the relationship between offset angles ($\theta_{XZ}$, $\theta_{YZ}$) and Euler angles ($\phi$, $\theta$) are shown schematically in Figure 3a. However, eq 11 has a limited application to biaxial orientation distributions in the $Y-Z$ plane, since a low $I_c(\theta_{XZ})$ value at an angle $\theta_{XZ}$ close to 90° may lead miscalculation of the function $I_c(\phi, \theta)$ when both angles $\phi$ and $\theta$ are close to 90°. If the distribution in the $X-Z$ plane is narrow, the relationship shown in Figure 3a may be replaced by an approximation in Figure 3b. The offset and Euler angles can be correlated with each other by

$$\theta_{YZ} = \tan^{-1}(\sin\phi \tan\theta) \quad (12)$$

$$\theta_{XZ} = \sin^{-1}(\cos\phi \sin\theta) \quad (13)$$

The distribution function $I_c(\phi, \theta)$ can be calculated by combining eqs 11−13, once the functions $I_c(\theta_{XZ})$ and $I_c(\theta_{YZ})$ have been determined by WAXD.

**2.2.3. Birefringence Measurements.** The birefringence of the BO−PLLA film was measured using a transmission optical microscope (BH-2, Olympus) fitted with a ×20 objective lens. Polarized monochromatic light ($\lambda = 589$ nm) was chosen as a light source. The BO−PLLA film was sandwiched between a glass slide and a cover glass on the sample stage, and a Berek compensator was used for the measurement of the sample birefringence between the sample *Y* axis and *Z* axis directions, $\Delta n_{YZ}$.

The sample birefringence $\Delta n_{YZ}$ can be related[15] to the coefficient $P_{200}$ determined by birefringence measurement, $P_{200}^{B}$, by

$$\Delta n_{YZ} = P_{200}^{B} \Delta n_o \quad (14)$$

where $\Delta n_o$ is the intrinsic birefringence for the material and

$$\Delta n_o = \chi_c \Delta n_c + (1 - \chi_c)\Delta n_a \quad (15)$$

where $\Delta n_c$ and $\Delta n_a$ are the values of intrinsic birefringence for the crystalline and amorphous regions of PLLA, which are reported[14] to be 0.0207 and 0.0587, respectively.

## 3. Results and Discussion

**3.1. Polarized Raman Spectroscopy.** Figure 4 shows polarized Raman spectra for the BO−PLLA film obtained for different polarization scattering geometries. In Figure 4b, different polarized Raman scattering intensities for the *Y*(*ZZ*)*Y* and *Y*(*XX*)*Y* geometries were observed for both Raman bands at 926 and 875 $cm^{-1}$. This indicates the presence of anisotropy of Raman polarizability in the film. The anisotropy of polarized Raman scattering can be seen more clearly in Table 3, which quantifies the polarized Raman scattering intensities for Raman bands at 926 and 875 $cm^{-1}$ for the different polarization scattering geometries. Using eq 2, the orientation distribution coefficients ($P_{lm0}$) were determined for each Raman band. Subsequently, the values $P_{lm0}$ for the Raman bands at 926 and 875 $cm^{-1}$ were corrected for their tilt angle using eq 3 in order to obtain the molecular orientation distribution coefficients for the crystalline regions only ($P_{lm0,c}$) and for an average over the crystalline and amorphous regions ($P_{lm0,chain}$). Once both coefficients $P_{lm0,c}$ and $P_{lm0,chain}$ were determined, the orientation distribution coefficients for the amorphous regions ($P_{lm0,a}$) could be estimated using eqs 4 and 5. All of the calculated coefficients for the BO−PLLA film are summarized in Tables 4 and 5. A relatively large standard deviation of the $P_{200}$ value for the 926 $cm^{-1}$ band is due probably to an error of intensity measurements for the weak Raman band.

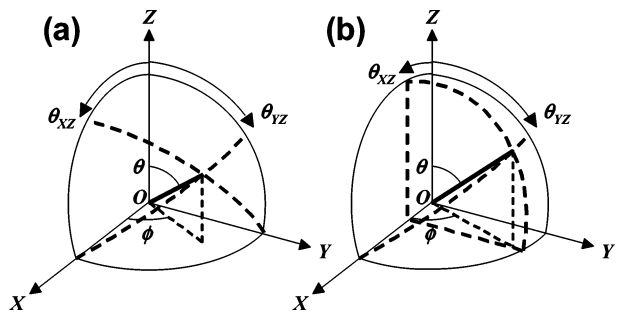


**Figure 3.** (a) Relationships between offset angles ($\theta_{XZ}$, $\theta_{YZ}$) and Euler angles ($\phi$, $\theta$), and (b) with an approximation under the condition where the angle $\theta_{XZ}$ is small.

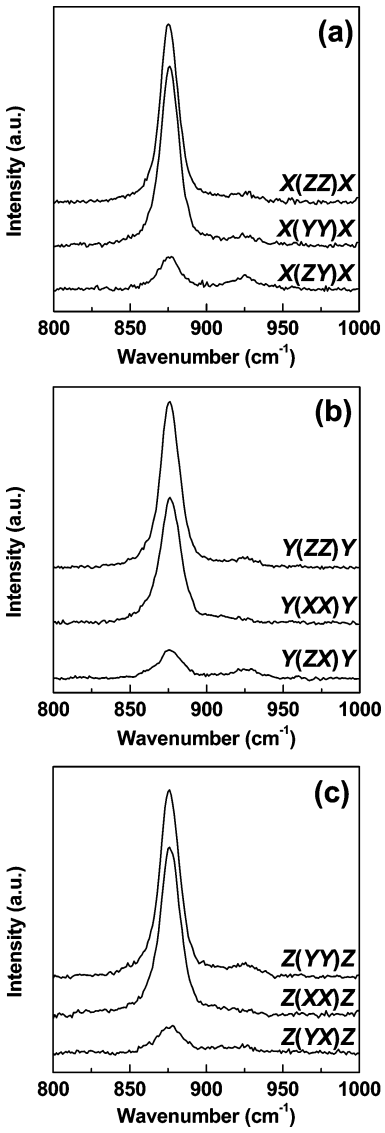


**Figure 4.** Polarized Raman spectra for the BO−PLLA film: (a) through, (b) edge, and (c) end.

Using eqs 7 and 8, coefficients $A_{lm0}^{mp}$ in the most probably molecular orientation distribution function for the BO−PLLA film were calculated for the crystalline regions only, $N_{mp,c}(\phi, \theta)$, and for the amorphous regions only, $N_{mp,a}(\phi, \theta)$. As described in the Experimental Section, the values $A_{200}^{mp}$, $A_{220}^{mp}$, and $A_{400}^{mp}$ were estimated in the first step of the calculation followed by the determination of the values $A_{420}^{mp}$ and $A_{440}^{mp}$ in the second step, and the results are given in Table 6.

Once all of the values $A_{lm0}^{mp}$ were known, the functions $N_{mp,c}(\phi, \theta)$ and $N_{mp,a}(\phi, \theta)$ could be determined using a cylindrical coordinate system,[18,29] $\phi-\theta-N_{mp}(\phi, \theta)$, as shown in Figure 5. Both the functions $N_{mp,c}(\phi, \theta)$ and $N_{mp,a}(\phi, \theta)$ have been normalized in the figure so that the volume of each distribution function equals to unity. The molecular orientation distribution in the crystalline regions of the BO−PLLA (Figure 5a) was predominantly uniaxial in the direction $(\phi, \theta) = (0°, 0°)$, which corresponds to the sample *Z* axis. In addition, the function $N_{mp,c}(\phi, \theta)$ spreads toward the direction $(\phi, \theta) = (90°, 90°)$, which corresponds to the sample *Y* axis and concentrates in the regions around $\phi = 90°$. These observations indicated that the molecules in the crystalline regions of the BO−PLLA

**Table 3.** Polarized Raman Scattering Intensities for Different Polarization Scattering geometries for the BO−PLLA Film after normalization ($\sum \alpha'_{ZZ}{}^2 = 100$)

| Raman band (cm-1) | $\sum \alpha'_{XX}{}^2$ | $\sum \alpha'_{YY}{}^2$ | $\sum \alpha'_{ZZ}{}^2$ | $\sum \alpha'_{YZ}{}^2$ | $\sum \alpha'_{ZX}{}^2$ | $\sum \alpha'_{XY}{}^2$ | $R_N$ (%) |
|---|---|---|---|---|---|---|---|
| 926 | 26 ± 6 | 85 ± 11 | 100 ± 20 | 111 ± 19 | 118 ± 7 | 51 ± 25 | 17 |
| 875 | 65 ± 2 | 85 ± 2 | 100 ± 1 | 16 ± 0.2 | 15 ± 1 | 11 ± 0.2 | 1 |

**Table 4.** Orientation Distribution Coefficients ($P_{lm0}$) for Raman Bands at 926 and 875 $cm^{-1}$ Determined for the BO−PLLA Film

| Raman band ($cm^{-1}$) | assignment[a] | $P_{200}$ | $P_{220}$ | $P_{400}$ | $P_{420}$ | $P_{440}$ |
|---|---|---|---|---|---|---|
| 926 | C | 0.56 ± 0.22 | −0.07 ± 0.02 | 0.25 ± 0.09 | −0.01 ± 0.002 | 0.01 ± 0.007 |
| 875 | C+A | 0.10 ± 0.006 | −0.02 ± 0.003 | −0.06 ± 0.02 | 0 ± 0.002 | 0 ± 0.0003 |

[a] C, Raman band assigned to the crystalline region only; C + A, Raman band assigned to both the crystalline and amorphous regions.

**Table 5.** Molecular Orientation Distribution Coefficients for the Crystalline Regions Only ($P_{lm0,c}$), for an Average of the Crystalline and Amorphous Regions ($P_{lm0,chain}$) and for the Amorphous Regions Only ($P_{lm0,a}$) for the BO−PLLA Film

| | $P_{200}$ | $P_{220}$ | $P_{400}$ | $P_{420}$ | $P_{440}$ |
|---|---|---|---|---|---|
| $P_{lm0,c}$ | 0.56 ± 0.11 | −0.07 ± 0.01 | 0.25 ± 0.04 | −0.01 ± 0.001 | 0.01 ± 0.004 |
| $P_{lm0,chain}$ | 0.25 ± 0.02 | −0.05 ± 0.01 | 0.19 ± 0.05 | 0 ± 0.005 | 0 ± 0.001 |
| $P_{lm0,a}$ | 0.06 ± 0.03 | −0.03 ± 0.01 | −0.02 ± 0.05 | 0 | 0 |

**Table 6.** Coefficients $A_{lm0}^{mp}$ in the Most Probable Molecular Orientation Distribution functions for the BO−PLLA Film

| | step | $A_{200}^{mp}$ | $A_{220}^{mp}$ | $A_{400}^{mp}$ | $A_{420}^{mp}$ | $A_{440}^{mp}$ | $R_A$ (%) |
|---|---|---|---|---|---|---|---|
| $N_{mp,c}(\phi, \theta)$ | first | 17.8 | −96.2 | −0.5 | | | 0.1 |
| | second | | | | 28.4 | −19.9 | 0.1 |
| $N_{mp,a}(\phi, \theta)$ | first only | 1.3 | −7.9 | 0.2 | | | 0.1 |

film were highly oriented in the sample $Y-Z$ plane with their preferential orientation in the direction of the $Z$ axis.

The molecular orientation distribution in the amorphous regions of the BO−PLLA film in Figure 5b is, on the other hand, found to be flatter than the function $N_{mp,c}(\phi, \theta)$, which indicates that the molecules in the amorphous regions are oriented less than in the crystalline regions. The function $N_{mp,a}(\phi, \theta)$ shows no molecular orientation around the axis $(\phi, \theta) = (0°, 90°)$, which corresponds to the sample $X$ axis, similarly observed for the function $N_{mp,c}(\phi, \theta)$. Although the function $N_{mp,a}(\phi, \theta)$ decreases monotonically toward the direction $(\phi, \theta) = (0°, 90°)$, no significant change is observed toward the $(\phi, \theta) = (0°, \pm 90°)$ directions. These results indicated that the molecules in the amorphous regions were oriented biaxially in the $Y-Z$ plane without any unidirectional orientation, and the molecular orientation distribution for the $Y-Z$ plane in the amorphous regions was considerably broader than in the crystalline regions.

**3.2. Comparison with WAXD Analysis.** Figure 6 shows the intensity of the Bragg peaks for the (0 0 10) plane in the $X-Z$ direction and for the (2 0 0)/(1 1 0) planes in the $Y-Z$ direction of the PLLA α-form crystals in the BO−PLLA film. The discrete and continuous intensity profiles of $I_c(\theta_{XZ})$ and $I_c(\theta_{YZ})$, respectively, are a result of using different techniques to measure their intensity as described in the Experimental Section. Both the diffraction intensity profiles $I_c(\theta_{XZ})$ and $I_c(\theta_{YZ})$ show a peak at $\theta_{XZ} = \theta_{YZ} = 0°$. This indicates that PLLA crystallites are oriented preferentially toward the sample $Z$ axis in both the $X-Z$ and $Y-Z$ planes. The orientation distribution of the crystallites $I_c(\phi, \theta)$ in the BO−PLLA film was determined using eq 11 and the angular relationships given in eqs 12 and 13 as shown in Figure 7.

PLLA crystallites were found to be oriented predominantly in the direction of $(\phi, \theta) = (0°, 0°)$, that is, in the direction of the sample $Z$ axis. With regard to the $X-Y$ plane, on the other hand, the crystallites show preferential orientation in the $Y$-axis direction. Although a slight asymmetry is observed with respect to the sample $X-Z$ plane, the orientation distribution function

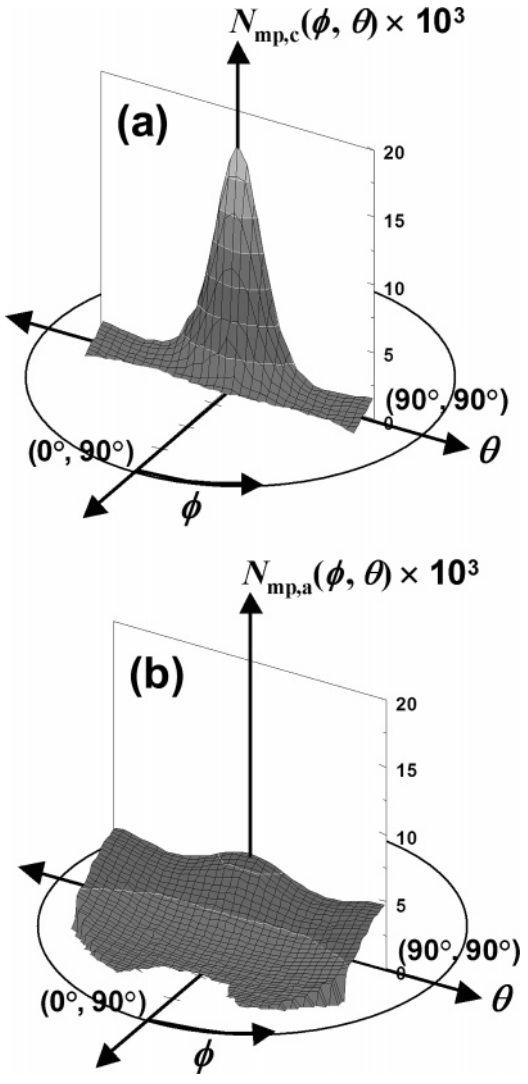


**Figure 5.** Most probable molecular orientation distribution functions for the (a) crystalline and (b) amorphous regions only of the BO−PLLA film. Axes along $(\phi, \theta) = (0°, 90°)$, $(90°, 90°)$, and $(0°, 0°)$ correspond to the sample $X$, $Y$, and $Z$ axes, respectively.

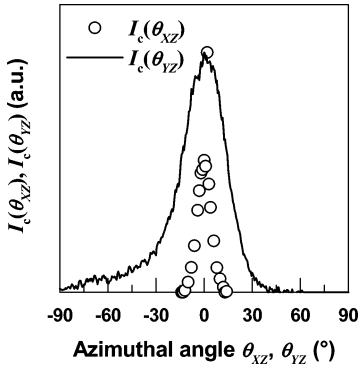


**Figure 6.** Bragg peaks for the (0 0 10) plane in the $X-Z$ direction and the (2 0 0)/(1 1 0) planes in the $Y-Z$ direction of PLLA α-form crystals in the BO−PLLA film.

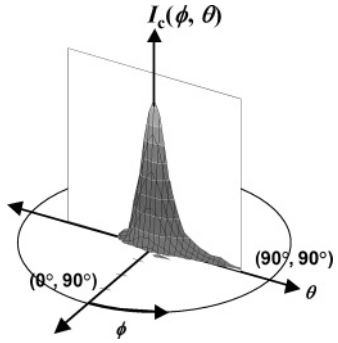


**Figure 7.** Orientation distribution function for crystallites $I_c(\phi, \theta)$ in the BO−PLLA film determined by WAXD. $(\phi, \theta) = (0°, 90°)$, (90°, 90°), and (0°, 0°) correspond to the sample $X$, $Y$, and $Z$ axes, respectively.

**Table 7.** Values of the Full Width at Half Maximum (fwhm) for the Orientation Distribution Functions $N_{mp,c}(\phi, \theta)$ and $I_c(\phi, \theta)$ in the Sample $X-Z$ and $Y-Z$ Planes of the BO−PLLA Film

| | fwhm (°) | |
|---|---|---|
| | $X-Z$ plane | $Y-Z$ plane |
| $N_{mp,c}(\phi, \theta)$ | 13 | 30 |
| $I_c(\phi, \theta)$ | 8 | 27 |

of the crystallites in the BO−PLLA film shows reasonable agreement with the molecular orientation distribution in the crystalline regions determined by polarized Raman spectroscopy (Figure 5a). As a quantitative measure of the orientation distribution of the crystallites in the $X-Z$ and $Y-Z$ planes, the full widths at half-maximum (fwhm) were calculated for directions $\phi = 0°$ and 90° for $I_c(\phi, \theta)$ in Figure 7 and are compared with those for the function $N_{mp,c}(\phi, \theta)$ in Table 7. The values of fwhm obtained by WAXD are found to be consistent with those determined by polarized Raman spectroscopy for both planes, which suggests that the function $N_{mp,c}(\phi, \theta)$ is useful for the study of orientation distributions of crystallites.

**3.3. Comparison with Sample Birefringence.** The sample birefringence for the $Y-Z$ plane $\Delta n_{YZ}$ of the BO−PLLA film was measured to be $9.3 \pm 0.2 \times 10^{-3}$, which gives a value of the coefficient $P_{200}^{B}$ in eq 14 of 0.23. This value is comparable to the $P_{200,chain}$ value of 0.25 shown in Table 5, since both coefficients are quantitative measurements of the molecular orientation distribution for an average over the crystalline and amorphous regions of the BO−PLLA film.

**3.4. Development of Molecular Orientation in the Crystalline and Amorphous Regions.** A number of studies[34−37] have reported that the molecular orientation in the crystalline regions tends to be higher than in the amorphous regions as a result of biaxial drawing of polymer samples. The anisotropy of the molecular orientation distribution in the amorphous regions, however, followed that in the crystalline regions in these studies. It is significant to note that different levels of orientation in the crystalline and amorphous regions were observed for the current BO−PLLA film. Two possible reasons could explain the difference with respect to the film forming process.

First, the amorphous regions would behave[38] like a rubber following affine deformation when the film is drawn at a temperature above its glass transition temperature ($T_g$). A stress concentration will develop in the molecules in the crystalline regions and intercrystalline tie molecules. The stresses on the crystalline regions would lead to intracrystallite slip and crystallite rotation,[39−41] which would result in the reorientation of crystallites.[14] Since it is known[39,41] that the occurrence of the crystallite slip depends on the critical resolved shear stress on the slip plane, the molecular orientation in the crystalline regions would be more sensitive to the stress state than in the amorphous regions undergoing affine deformation. Second, the stresses built in the molecules in the amorphous regions would be released, particularly at high temperature, by orientation relaxation.[2,42,43] The orientation distributions shown in Figure 5 suggest in the film formation process that the film was initially drawn biaxially at a temperature above $T_g$ with a higher stress along the $Z$ axis than along the $Y$ axis. The difference of molecular orientation distributions in the crystalline and amorphous regions is, therefore, considered to be due to the nature of the molecules in both regions. The molecules in the crystalline regions are fixed in position below the crystal melting point, whereas those in the amorphous regions can relax above their $T_g$.

## 4. Conclusions

Molecular orientation distributions in the crystalline and amorphous regions of a BO−PLLA film were studied fully by means of polarized Raman spectroscopy. Assuming that Raman tensors of PLLA have cylindrical symmetry, it was possible to determine the molecular orientation distribution coefficients from Raman spectra for the backscattering geometry only.

The Raman band at 926 $cm^{-1}$ was chosen for the study of the molecular orientation distribution in the crystalline regions only. The most probable molecular orientation distribution function for the crystalline regions $N_{mp,c}(\phi, \theta)$ of the BO−PLLA film showed that PLLA molecules were oriented biaxially in the sample $Y-Z$ plane with predominant orientation toward the $Z$ axis, which was consistent with the orientation distribution of PLLA crystallites determined by WAXD.

Similarly, the Raman band at 875 $cm^{-1}$ was employed for the study of the molecular orientation distribution averaged over the crystalline and amorphous regions. The orientation distribution of the Raman tensor was corrected for its tilt angle Ω, which enabled the function $N_{mp,chain}(\phi, \theta)$ to be determined. A similar result was obtained from birefringence measurements.

Furthermore, the molecular orientation distribution coefficients for the amorphous regions only ($P_{lm0,a}$) of the BO−PLLA could be calculated from the coefficients $P_{lm0,c}$ and $P_{lm0,chain}$. By comparing the function $N_{mp,a}(\phi, \theta)$ with $N_{mp,c}(\phi, \theta)$, the molecular orientation distribution in the amorphous regions only was found to be biaxial in the $Y-Z$ plane, although the distribution in the $X-Z$ plane was broad with no predominant orientation toward the $Z$ axis. The difference of molecular orientation in the crystalline and amorphous regions in the BO−

PLLA film was considered to be due to different deformation mechanisms in each regions and relaxation of the amorphous regions during the film processing.

Future work will study the relationships between the microstructure of BO−PLLA films, prepared using different processing conditions, and its influence upon the mechanical properties and degradation behavior of the films.

## Appendix

**Determination of the Polarized Raman Scattering Intensities for Different Polarization Scattering Geometries.** In this study, the polarized Raman spectra were obtained from three different cross-sections of the film. Although the backscattering geometry was used for all of the measurements, the scattering volume may vary owing to the nature of each sample. The following factors may be considered in order to normalize the polarized Raman scattering intensities for different polarization scattering geometries measured from different samples. If the normalized values of $\sum \alpha'_{IJ}{}^2$ are given as $(\sum \alpha'_{IJ}{}^2)_N$, the scattering intensities in Table 2 can be correlated by

$$S_1(\sum \alpha'_{ZZ}{}^2)_{through} = S_2(\sum \alpha'_{ZZ}{}^2)_{edge} = (\sum \alpha'_{ZZ}{}^2)_N \quad (A1)$$

$$S_1(\sum \alpha'_{YY}{}^2)_{through} = S_3(\sum \alpha'_{YY}{}^2)_{end} = (\sum \alpha'_{YY}{}^2)_N \quad (A2)$$

$$S_2(\sum \alpha'_{XX}{}^2)_{edge} = S_3(\sum \alpha'_{XX}{}^2)_{end} = (\sum \alpha'_{XX}{}^2)_N \quad (A3)$$

where $S_1$, $S_2$, and $S_3$ are correlation factors for the polarized Raman scattering intensities obtained from the through, edge, and end samples, respectively. It is, however, difficult to solve one set of ($S_1$, $S_2$, $S_3$) values from the values $\sum \alpha'_{IJ}{}^2$ measured experimentally. For a given set of ($S'_1$, $S'_2$, $S'_3$) values, error coefficients may be defined for eqs A1−A3 by

$$R_1 = \frac{[S'_1(\sum \alpha'_{ZZ}{}^2)_{through} - S'_2(\sum \alpha'_{ZZ}{}^2)_{edge}]^2}{\left[\frac{S'_1(\sum \alpha'_{ZZ}{}^2)_{through} + S'_2(\sum \alpha'_{ZZ}{}^2)_{edge}}{2}\right]^2} \quad (A4)$$

$$R_2 = \frac{[S'_1(\sum \alpha'_{YY}{}^2)_{through} - S'_3(\sum \alpha'_{YY}{}^2)_{end}]^2}{\left[\frac{S'_1(\sum \alpha'_{YY}{}^2)_{through} + S'_3(\sum \alpha'_{YY}{}^2)_{end}}{2}\right]^2} \quad (A5)$$

$$R_3 = \frac{[S'_2(\sum \alpha'_{XX}{}^2)_{edge} - S'_3(\sum \alpha'_{XX}{}^2)_{end}]^2}{\left[\frac{S'_2(\sum \alpha'_{XX}{}^2)_{edge} + S'_3(\sum \alpha'_{XX}{}^2)_{end}}{2}\right]^2} \quad (A6)$$

and factors $S'_i$ can be chosen by numerical calculations to give the same amount of errors between the intensity correlations, hence

$$R_1 = R_2 = R_3 \quad (A7)$$

The error caused by the normalization process is given by

$$R_N = \frac{|S'_1(\sum \alpha'_{ZZ}{}^2)_N - (\sum \alpha'_{ZZ}{}^2)_N|}{(\sum \alpha'_{ZZ}{}^2)_N} = \frac{\sqrt{R_1}}{2} \quad (A8)$$

The polarized Raman scattering intensities after the normalization $(\sum \alpha'_{IJ}{}^2)_N$ can be defined using factors $S'_i$ by

$$(\sum \alpha'_{XX}{}^2)_N = \frac{S'_2(\sum \alpha'_{XX}{}^2)_{edge} + S'_3(\sum \alpha'_{XX}{}^2)_{end}}{2} \quad (A9)$$

$$(\sum \alpha'_{YY}{}^2)_N = \frac{S'_1(\sum \alpha'_{YY}{}^2)_{through} + S'_3(\sum \alpha'_{YY}{}^2)_{end}}{2} \quad (A10)$$

$$(\sum \alpha'_{ZZ}{}^2)_N = \frac{S'_1(\sum \alpha'_{ZZ}{}^2)_{through} + S'_2(\sum \alpha'_{ZZ}{}^2)_{edge}}{2} \quad (A11)$$

$$(\sum \alpha'_{ZZ}{}^2)_N = S'_1(\sum \alpha'_{YZ}{}^2)_{through} \quad (A12)$$

$$(\sum \alpha'_{ZX}{}^2)_N = S'_2(\sum \alpha'_{ZX}{}^2)_{edge} \quad (A13)$$

$$(\sum \alpha'_{XY}{}^2)_N = S'_3(\sum \alpha'_{XY}{}^2)_{end} \quad (A14)$$

A program was written using a Solver function in Microsoft Excel software to calculate the values $S'_i$ in eqs A9−A14 under the constraint of eq A7.

**Acknowledgment.** We thank Mitsubishi Plastics for the supply of the material. The work was supported by Four Square, a Division of Mars U.K. Ltd. One of the authors (M.T.) is grateful to Universities U.K. for financial support through the ORS scheme (ORS/2000028028).

## References and Notes

(1) Smith, P. B.; Leugers, A.; Kang, S.; Yang, X.; Hsu, S. L. *Macromol. Symp.* **2001**, *175*, 81−94.
(2) Smith, P. B.; Leugers, A.; Kang, S.; Hsu, S. L.; Yang, X. *J. Appl. Polym. Sci.* **2001**, *82*, 2497−2505.
(3) Kikkawa, Y.; Abe, H.; Iwata, T.; Inoue, Y.; Doi, Y. *Biomacromolecules* **2002**, *3*, 350−356.
(4) Tsuji, H.; Ogiwara, M.; Saha, S. K.; Sakaki, T. *Biomacromolecules* **2006**, *7*, 380−387.
(5) Tsuji, H.; Ikada, Y. *J. Polym. Sci., Part A: Polym. Chem.* **1998**, *36*, 59−66.
(6) Orchard, G. A. J.; Spiby, P.; Ward, I. M. *J. Polym. Sci., Part B: Polym. Phys.* **1990**, *28*, 603−621.
(7) Di Maio, L.; Scarfato, P.; Incarnato, L.; Acierno, D. *Macromol. Symp.* **2002**, *180*, 1−8.
(8) Bower, D. I. *J. Polym. Sci.: Polym. Phys. Ed.* **1972**, *10*, 2135−2153.
(9) Sourisseau, C. *Chem. Rev.* **2004**, *104*, 3851−3891.
(10) Tanaka, M.; Young, R. J. *J. Mater. Sci.* **2006**, *41*, 963−991.
(11) Maxfield, J.; Stein, R. S.; Chen, M. C. *J. Polym. Sci.: Polym. Phys. Ed.* **1978**, *16*, 37−48.
(12) Pigeon, M.; Prud'homme, R. E.; Pezolet, M. *Macromolecules* **1991**, *24*, 5687−5694.
(13) Tanaka, M.; Young, R. J. *J. Macromol. Sci. Phys.-B* **2005**, *44*, 967−991.
(14) Tanaka, M.; Young, R. J. *Macromolecules* **2006**, *39*, 3312−3321.
(15) Yang, S.; Michielsen, S. *Macromolecules* **2002**, *35*, 10108−10113.
(16) Rousseau, M.-E.; Lefevre, T.; Beaulieu, L.; Asakura, T.; Pezolet, M. *Biomacromolecules* **2004**, *5*, 2247−2257.
(17) Jarvis, D. A.; Hutchinson, I. J.; Bower, D. I.; Ward, I. M. *Polymer* **1980**, *21*, 41−54.
(18) Bower, D. I. *Polymer* **1982**, *23*, 1251−1255.
(19) Lapersonne, P.; Bower, D. I.; Ward, I. M. *Polymer* **1992**, *33*, 1266−1276.
(20) Bower, D. I. *J. Phys. B: Atom. Mol. Phys.* **1976**, *9*, 3275−3293.
(21) Kobayashi, J.; Asahi, T.; Ichiki, M.; Oikawa, A.; Suzuki, H.; Watanabe, T.; Fukada, E.; Shikinami, Y. *J. Appl. Phys.* **1995**, *77*, 2957−2973.
(22) Fischer, E. W.; Sterzel, H. J.; Wegner, G. *Kolloid-Z. (u) Z. Polym.* **1973**, *251*, 980−990.
(23) Bunge, H.-J.; Roberts, W. T. *J. Appl. Crystallogr.* **1969**, *2*, 116−128.
(24) Roe, R.-J. *J. Polym. Sci., Part A-2* **1970**, *8*, 1187−1194.
(25) Purvis, J.; Bower, D. I. *J. Polym. Sci.: Polym. Phys. Ed.* **1976**, *14*, 1461−1484.

(26) Yang, S.; Michielsen, S. *Macromolecules* **2003**, *36*, 6484−6492.
(27) Damen, T. C.; Porto, S. P. S.; Tell, B. *Phys. Rev.* **1966**, *142*, 570−574.
(28) Nomura, S.; Nakamura, N.; Kawai, H. *J. Polym. Sci., Part A-2* **1971**, *9*, 407−420.
(29) Bower, D. I.; Jarvis, D. A.; Ward, I. M. *J. Polym. Sci., Part B: Polym. Phys.* **1986**, *24*, 1459−1479.
(30) Bremard, C.; Dhamelincourt, P.; Laureyns, J.; Turrell, G. *Appl. Spectrosc.* **1985**, *39*, 1036−1039.
(31) Bremard, C.; Laureyns, J.; Turrell, G. *Can. J. Spectrosc.* **1987**, *32*, 70−78.
(32) Everall, N. J. *Appl. Spectrosc.* **1998**, *52*, 1498−1504.
(33) Cartier, L.; Okihara, T.; Ikada, Y.; Tsuji, H.; Puiggali, J.; Lotz, B. *Polymer* **2000**, *41*, 8909−8919.
(34) Hammersley, A. The Fit2D Home Page, 2004 ESRF, www.esrf.fr/computing/scientific/FIT2D/.
(35) Strobel, J. M.; Nam, S. *J. Appl. Polym. Sci.* **1991**, *42*, 159−168.
(36) Taraiya, A. K.; Orchard, G. A. J.; Ward, I. M. *J. Polym. Sci., Part B: Polym. Phys.* **1993**, *31*, 641−645.
(37) Karacan, I.; Taraiya, A. K.; Bower, D. I.; Ward, I. M. *Polymer* **1993**, *34*, 2691−2701.
(38) Botev, M.; Neffati, R.; Rault, J. *Polymer* **1999**, *40*, 5227−5232.
(39) Bowden P. B.; Young, R. J. *J. Mater. Sci.* **1974**, *9*, 2034−2051.
(40) Yamada, K.; Takayanagi, M. *J. Appl. Polym. Sci.* **1979**, *24*, 781−799.
(41) Lin, L.; Argon, A. S. *J. Mater. Sci.* **1994**, *29*, 294−323.
(42) Yamada, K.; Takayanagi, M. *J. Appl. Polym. Sci.* **1982**, *27*, 3479−3491.
(43) Yang, X.; Kang, S.; Yang, Y.; Aou, K.; Hsu, S. L. *Polymer* **2004**, *45*, 4241−4248.

BM060326L